Ore Geology Reviews 78 (2016) 268–280

Contents lists available at ScienceDirect

Ore Geology Reviews

journal homepage: www.elsevier.com/locate/oregeorev

# Molybdenite Re–Os and U–Pb zircon dating and genesis of the Dayana W-Mo deposit in eastern Ujumchin, Inner Mongolia

Anping Xiang [a,b,*], Yuchuan Chen [a], Leon Bagas [a,c], Hongquan She [a], Yongjian Kang [a], Wensheng Yang [a], Changjian Li [a]

[a] Institute of Mineral Resources, China Academy of Geology Sciences, Beijing 100037, China
[b] China University of Geosciences, Wuhan 430074, China
[c] Centre for Exploration Targeting, Centre of Excellence for Core to Crust Fluid Systems, University of Western Australia, 35 Stirling Highway, Crawley, Western Australia 6009, Perth, Australia

ARTICLE INFO

*Article history:*
Received 26 November 2015
Received in revised form 14 March 2016
Accepted 15 March 2016
Available online 22 March 2016

*Keywords:*
East Ujumchin
Inner Mongolia
Wolframite
Molybdenite
Geochronology
Quartz vein
Biotite monzogranite
LA-ICP-MS
Re–Os

ABSTRACT

The Dayana W-Mo deposit in eastern Ujumchin of Inner Mongolia is a quartz-vein type deposit in the mid-western part of the Central Asian Orogenic Belt (CAOB). Biotite monzogranite, quartz porphyry and hornfels host W-Mo in quartz veins. Based on spatial relationships, molybdenite was deposited first followed by wolframite. This contribution presents precise laser ablation inductively coupled plasma mass spectroscopy (LA-ICP-MS) U–Pb zircon dating and geochemical analysis of the biotite monzogranite. The U–Pb dating shows that the monzogranite is 134 ± 1 Ma. Major and trace element geochemistry shows that the monzogranite is characterized by high $SiO_2$ and $K_2O$ contents, a "Right-inclined" shape of the chondrite normalized REE patterns, enrichment of large ion lithophile elements (LILEs), and depletion of high field strength elements (HFSEs) such as Nb, P, Ba. The monzogranite is high-K calc-alkaline, has a strong negative Eu anomaly (Eu/Eu* = 0.04–0.45), low $P_2O_5$ content, high A/CNK of >1.2, enriched in large-ion lithophile elements (LILEs; such as Rb, Th, U, Nd, and Hf), and notably depleted in Ba, Sr, P, Ti, and Nb. These characteristics define the Dayana monzogranite as a highly fractionated peraluminous granite. Re–Os isotopic analysis of seven molybdenite samples from the deposit yield an isochron age of 133 ± 3 Ma (MSWD = 2.2), which indicates that the monzogranite and ore have the same age within error, are probably genetically related, and related to a major Early Cretaceous mineralizing event in China known as the Yanshanian.



## 1. Introduction

The Dayana W-Mo mineralization is located at East Ujumchin in Inner Mongolia (Fig. 1). The deposit is in the southwestern margin of the Greater Hinggan Mountain metallogenic belt (GHMMB; Fig. 1). Recent exploration in the belt has led to the discovery of numerous Cu, Mo, Fe, Pb, Zn, Au, Ag, and Ni polymetallic deposits, even though grasslands and forest cover the area. Deposits discovered include the Chaobuleng skarn Fe–Zn, Shamai W-bearing quartz-vein, Erdaohe skarn Pb–Zn(–Ag), Taipinggou porphyry-type Mo, Chalukou porphyry Mo(−Cu), Honghuaerji scheelite, and Duobaoshan porphyry Cu–Mo deposits (Mao and Wang, 1999; Mao et al., 2003a, 2011; Ge et al., 2007; Nie et al., 2010; Chen et al., 2008, 2011; Chen, 2010; Wu et al., 2011; She et al., 2012; Xiang et al., 2012, 2014; Li et al., 2013; Liu et al., 2013; Wang et al., 2015; Xu et al., 2015a,b; Jiang et al., in press).

Preliminary studies have recently led to the discovery of five outcropping high-grade W- and Mo-bearing quartz veins at Dayana (Fig. 2). This contribution is on this new discovery and reports on the geology, geochronology of mineralization and magmatism, and geochemical characteristics of the hosting rocks with the aim to better understand the genesis of mineralization in the GHMMB.

## 2. Regional geology

The Dayana W-Mo mineralization is in GHMMB located the Central Asian Orogenic Belt (CAOB) (Wilhem et al., 2012; Xu et al., 2015a,b; Wu et al., 2011;) between the Siberian Craton to the north and the North China Craton (NCC) to the south (Fig. 1). The Dongwuqi-Nenjiang belt is bound by the Elunchun Fault to the northwest and the Nenjiang Fault to the southeast (Fig. 1b), which is an area considered to rich in Au, Ag, Cu, Pb, Zn, Fe, Sn, and rare metallic metals (REE; Li, Be, Nb, Ta, and REE; Hong et al., 2003; She et al., 2012; Xu et al., 2015a,b). The tectonic evolution of the belt is complex and has been studied by many authors (Ge et al., 2005; Wu et al., 2011, 2015; Miao et al., 2007; Zhang et al., 2008; Chen, 2010; Wang et al., 2012; Sun et al., 2013; Gou et al., 2013; Xu et al., 2015a,b). In summary, these authors propose the following sequence of events: (1) suturing of the Erguna Block to the Xing'an Block during ca. 530–440 Ma; (2) closure of Paleo-Asian Ocean during ca. 330–280 Ma; (3) subduction of the

* Corresponding author at: Institute of Mineral Resources, China Academy of Geology Sciences, Beijing 100037, China.

http://dx.doi.org/10.1016/j.oregeorev.2016.03.012
0169-1368/

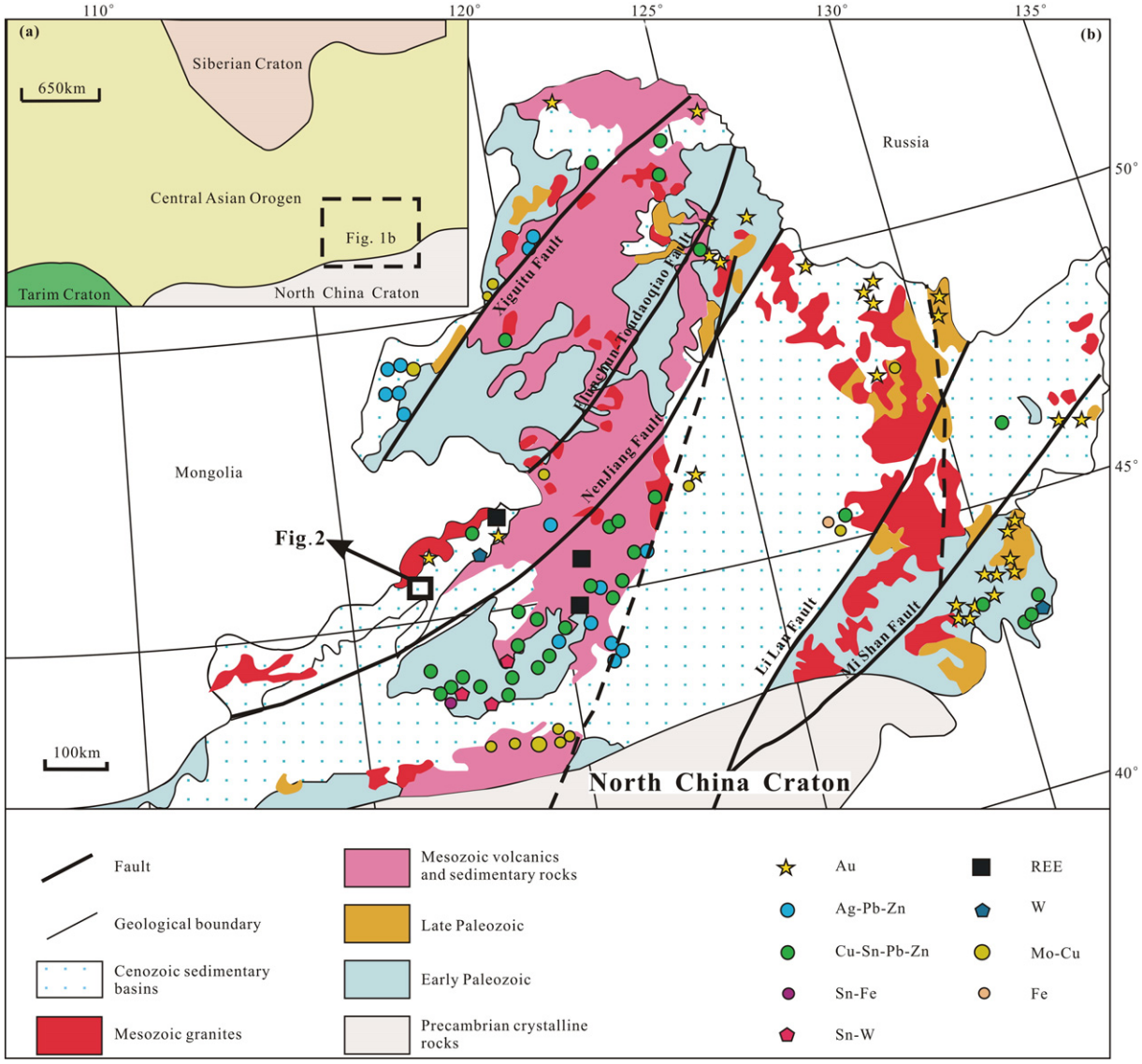


**Fig. 1.** Maps showing: (a) Relationship of study area with the Central Asian Orogen (Modified from Liu et al., 2016); (b) relationship of study area with the metallogenic belt in China (Modified from Liu et al., 2016).

Mongolia-Okhotsk Ocean during ca. 240–160 Ma resulting in collisional orogenic events and consequent post-collisional extensional collapse and magmatism; and (4) evolution of the Paleo-Pacific Ocean during ca. 150–120 Ma; and the oblique subduction of the Pacific Ocean since ca. 150 Ma.

The Dayana W-Mo deposit is located in the grasslands of Inner Mongolia and hosted by the poorly exposed Carboniferous-Permian Gegen'aobao Formation, which consists of andesite, andesitic pyroclastic rocks, dacite, siltstone, and thin beds of mudstone (Figs. 1, 2). An Early Cretaceous biotite monzogranite and a Cretaceous quartz porphyry dyke intrude the study area. The biotite monzogranite is part of the Dayana Granite and covers approximately 1 $km^2$ in area, and the quartz porphyry dyke crosses the monzogranite trending and some of the W-Mo mineralization (Fig. 2).

The northward-trending mineralized veins in the study area are hosted by northward-trending dextral faults, and are cut by eastward-trending sinistral faults. Both these faults appear to be associated with a NE-SW orientated compressional regime, which is parallel or subparallel to the quartz porphyry dyke. It is here proposed that the dyke was emplaced in the NE-SW orientated compressional regime shortly during the development of the faults and emplacement of the mineralized veins, suggesting that the quartz porphyry, mineralization and faults are broadly coeval.

## 3. Orebody characteristics

The biotite monzogranite in the Dayana Granite hosts mineralized quartz veins with hydrothermal alteration bordering the vein systems. The ore minerals include scheelite, molybdenite, chalcopyrite, native copper, pyrite and sphalerite, with gangue minerals including muscovite, quartz, beryl, K-feldspar, albite, and fluorite. The quartz veins have sharp boundaries with the biotite monzogranite.

### 3.1. Mineralization

Preliminary studies indicate that the mineralization at Dayana is situated towards the upper part of the biotite monzogranite and in faults along the contact between the monzogranite and country rocks. The mineralization appears to form a zonation from quartz-W veins to quartz-Mo veins (Fig. 3). Over 38 quartz-W veins and 65 quartz-Mo veins have been delineated to date.

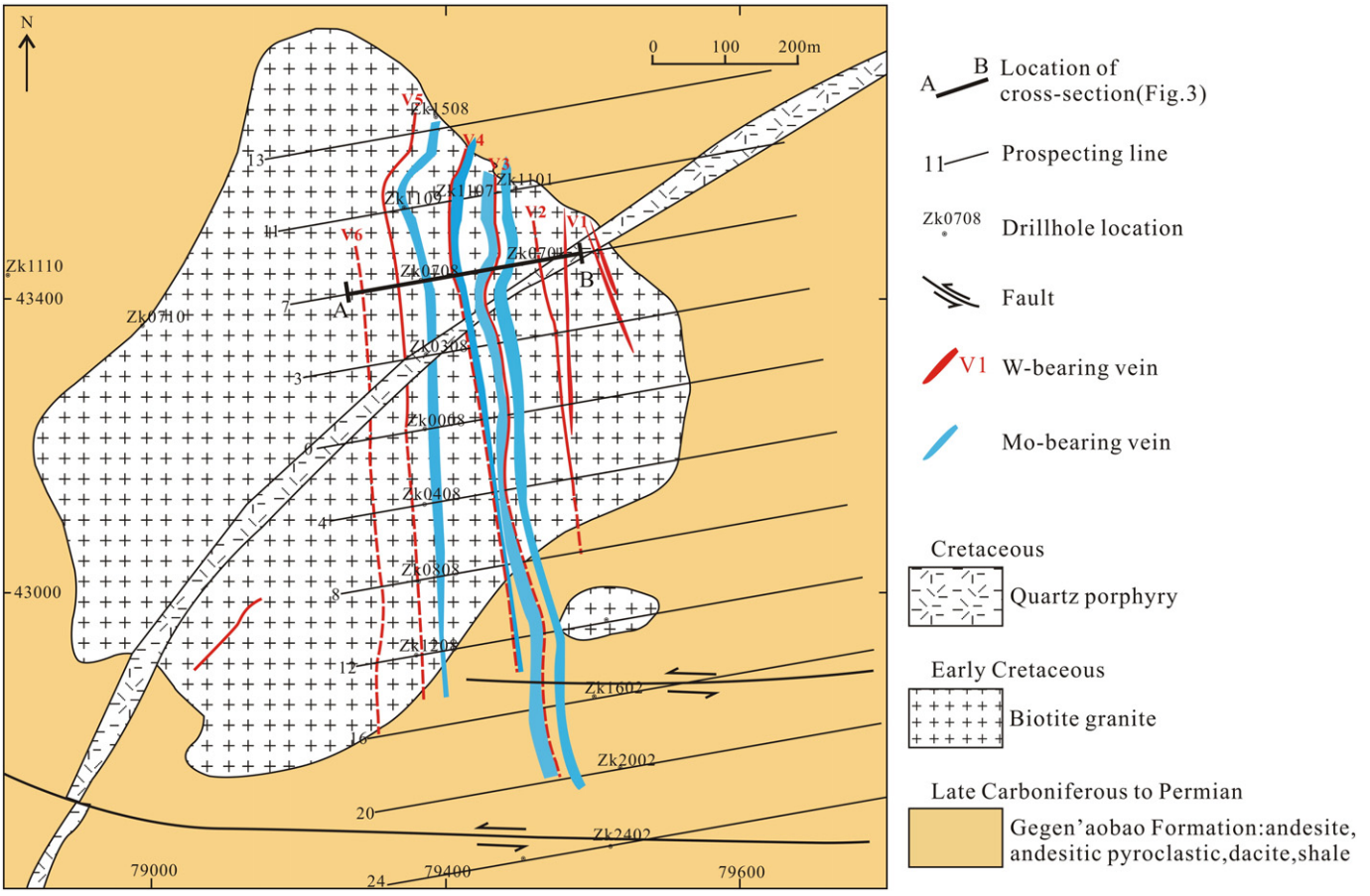


**Fig. 2.** Geological map of the Dayana W-Mo mineralization.

The mineralized quartz veins are subparallel to each other and the quartz porphyry dipping around 75° east cutting and the biotite monzogranite (Fig. 2). The longest mineralized vein is ~800 m long and 1 to 2 m wide. The richest quartz-W veins are located referred to as V3, V4 and V5, which are generally overlain by quartz-Mo veins (Figs. 2, 3). The mineralization extends to a depth of 300 m, but this observation is based on limited diamond-drilling and the mineralization remains open at depth (Fig. 3). The quartz-W mineralization is lenticular in shape and broadly consists of numerous radiating or densely distributed parallel 5 to 100 mm wide veins of $WO_3$ in the upper parts of large quartz veins. In detail, the mineralization in the WO3-bearing veins consists of large single crystals of varying diameters up to 50 mm across forming columns and needles in quartz (Fig. 4a,b). In addition, some veins of $WO_3$ are also located in the biotite monzogranite (Fig. 4). The overall grade of the vein is between 0.1 and 8.8%, $WO_3$ with an average grade of 0.81% $WO_3$. Examples of the mineralization in diamond-drillhole core are shown in Fig. 3.

The Mo mineralization is also widespread having a thicker width than the W mineralization, but more limited in number. The average grade on the Mo mineralization in the economic orebodies is ~0.12%.

Where both the Mo and W mineralization are present, the Mo occurs as sporadic disseminations in the country rock bordering quartz veins, along the edges of the quartz veins, and disseminated being intergrown with W in quartz–K-feldspar–muscovite veins interpreted to be magmatic in origin.

There is a recognizable difference between the Mo- and W-mineralized quartz veins. The quartz-Mo veins are commonly dark-coloured, accompanied by K-feldspar and muscovite suggestive of a pegmatitic association. These veins are often crosscut by white and transparent quartz-W veins with a greasy luster. The quartz of in the Mo-quartz veins is dark, and the Mo-quartz veins are fine and typically 1–5 mm in width with some veins being intersected by larger W-bearing veins. This relationship indicates that the molybdenite mineralization precedes the wolframite mineralization (Fig. 5).

### 3.2. Wall-rock alteration

Hydrothermal wall-rock alteration at Dayana is characterized by greisen and a mineral assemblage of silica, epidote, muscovite (up to 5 mm long), beryl, chlorite, K-feldspar, and albite. The Mo and W mineralization is commonly associated with greisen, albite, K-feldspar, and silica. Greisen containing narrow and densely distributed quartz-mica veins is present at the top of the biotite monzogranite in the Dayana Granite (Fig. 4d,i). Quartz-W veins, and the K-feldspar and albite alteration are synchronous, located at the lower levels of the veins (Fig. 4h), accompanied by wolframite and muscovite in some places (Fig. 4e), and locally surrounded by quartz-mica veins. Comb-shaped structures or re-cemented fractures are present in some of the quartz-W veins that are 10 mm to 2 m wide (Fig. 5b). The beryl forms 3–5 mm wide columnar crystals commonly between muscovite and quartz in the greisen (Fig. 4d).

Sericite, chlorite, and minor amounts of pyrite are common alteration minerals located along the edges of mineralized quartz veins. The outer parts of the alteration zone are characterized by the presence of biotite, indicative of hydrous potassic alteration.

## 4. Methods

### 4.1. U–Pb isotopic analysis

Two samples (DYN-19, DYN-30) of biotite monzogranite were collected for U–Pb zircon dating from diamond-drillhole (DDH) core at

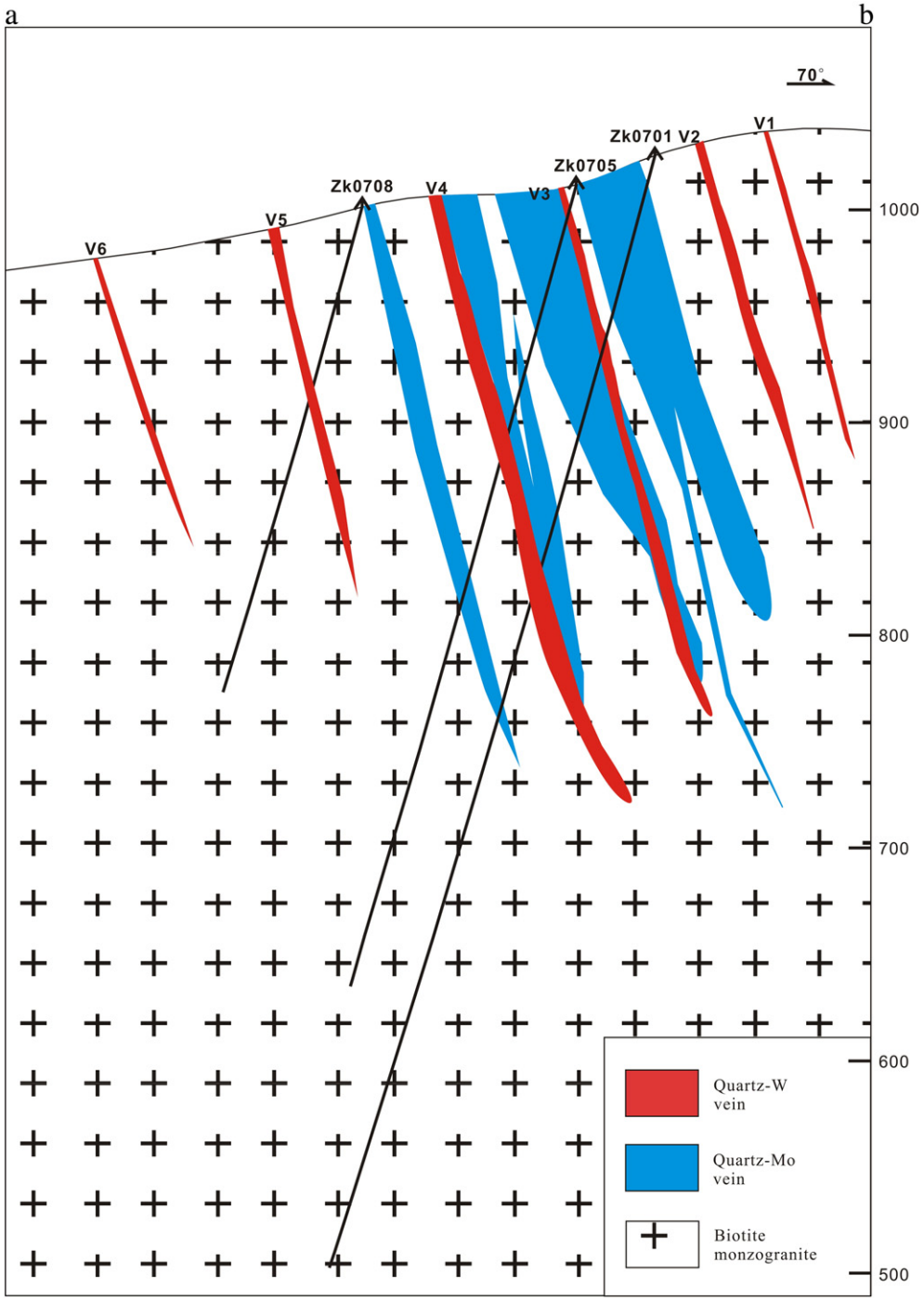


**Fig. 3.** Cross section showing the style of W-Mo mineralization at Davana.

the Dayana mineralization. Sample DYN-19 is from DDH ZK0705 at a depth of 110–112 m and DYN-30 is from DDH ZK1109 at a depth of 58–68 m. The samples were crushed and subjected to flotation and magnetic separation to obtain over 800 grains of zircons from both samples, which were mounted following the procedure outlined by Song et al. (2002). The procedure involved the selection of zircon grains with good crystal shapes and transparency using a binocular microscope. They were then placed on an epoxy surface for polishing, and examined for imperfections and inclusions using transmissive, reflective, and cathode luminescence (CL) images. The CL images were obtained using a LEO1450VP scanning electron microscope (SEM; 15 kV, 1.1 nA) at the Electronic Probe and Electron Microscope Laboratory of the Beijing Gaonian Pilot Technology Co. Ltd. A laser ablation inductively coupled plasma mass spectroscopy (LA-MC-ICP-MS) was used for U–Pb zircon dating at the MC-ICP-MS laboratory in the Institute of Mineral Resources of the Chinese Academy of Geological Sciences. The instrument used is a Finnigan Neptune MC-ICP-MS coupled with a New Wave UP-213 laser ablation system. Laser ablation was performed with a spot diameter of 25 μm, frequency of 10 Hz, and energy density of 2.5 J/cm$^2$ using He as the carrier gas. In order to ensure simultaneous reception of all target isotope signals and similarity of peak values of different mass numbers to obtain high-precision data, weak signals of $^{207}$Pb, $^{206}$Pb, $^{204}$Pb(+$^{204}$Hg), and $^{202}$Hg were recorded using a multi-ion counter, and the $^{208}$Pb, $^{232}$Th, and $^{238}$U signals were recorded using a Faraday cup. The measurement precision of homogeneous zircon grains for $^{207}$Pb/$^{206}$Pb, $^{206}$Pb/$^{238}$U, and $^{207}$Pb/$^{235}$U was approximately 2% (2σ),

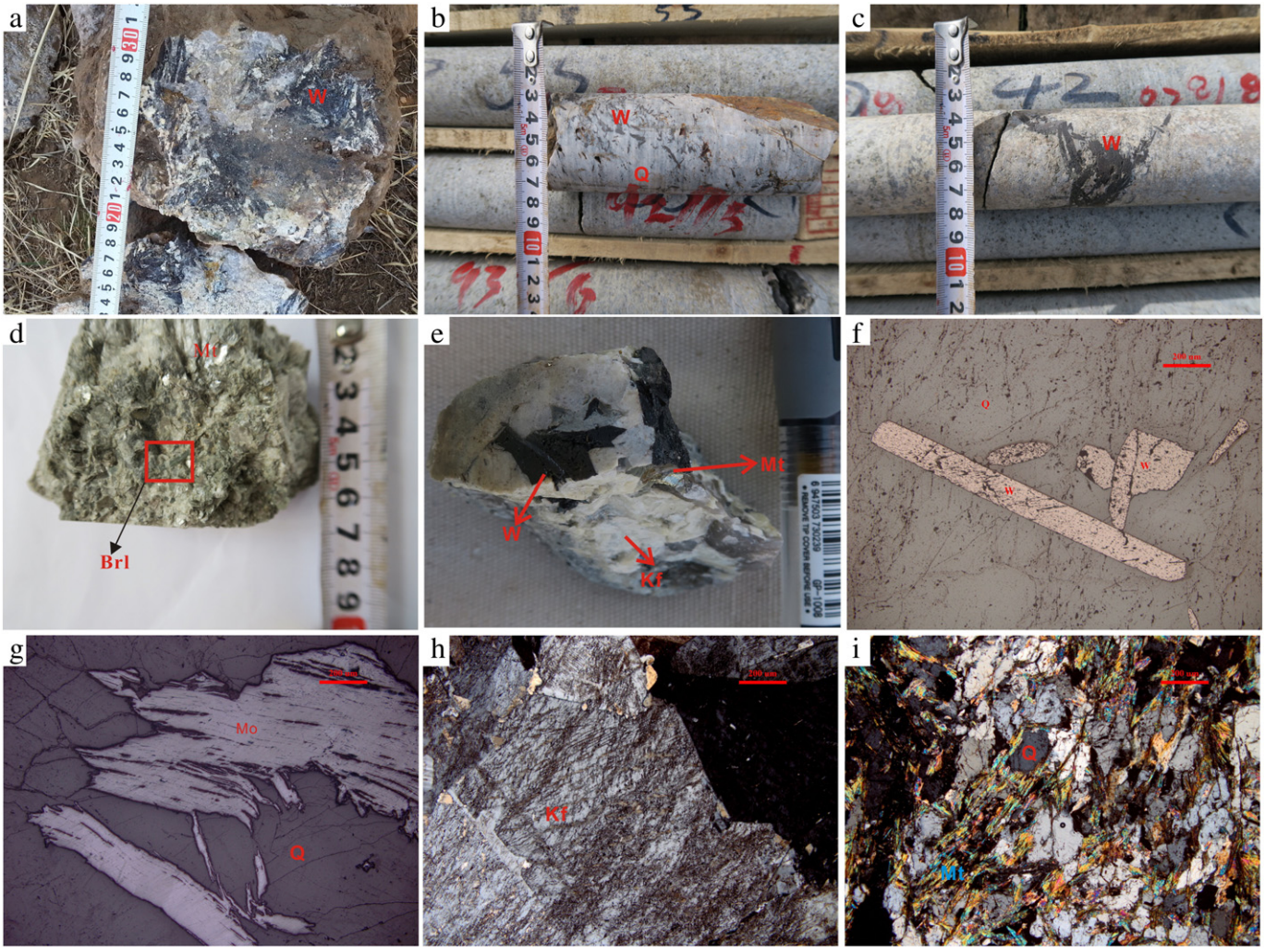


**Fig. 4.** Examples of the mineralization in diamond-drillhole core at Davana.

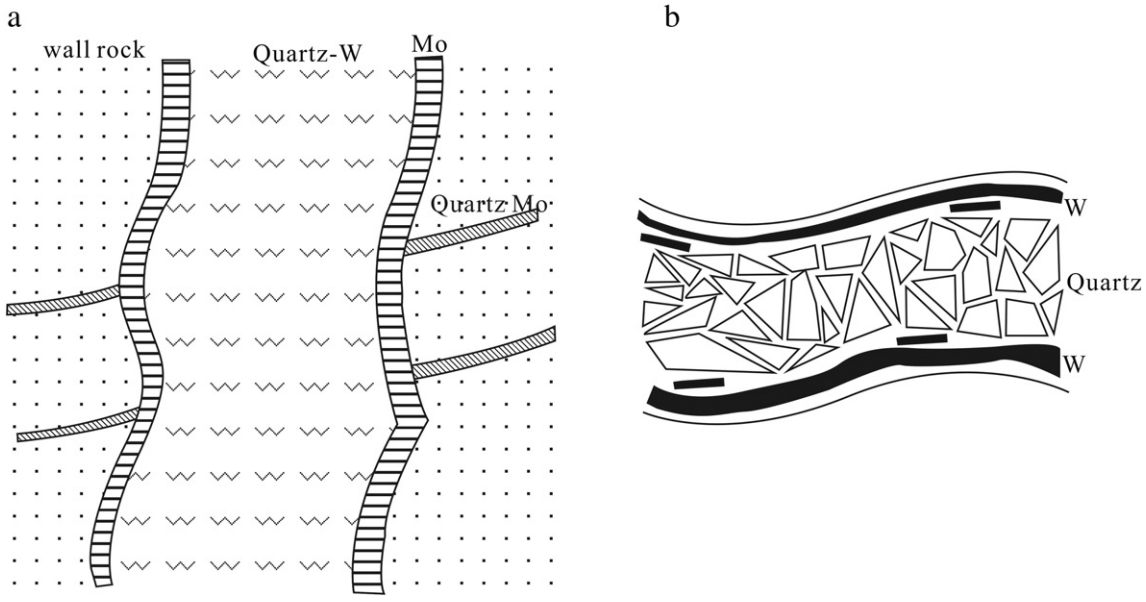


**Fig. 5.** (a) Relationship of W-veins with Mo-veins and Mo-mineralization. The Mo-veins are often cross by white and transparent quartz-W veins, and Mo-mineralization sporadically forms disseminations in the country rock bordering quartz veins. (b) Comb-shaped structures or re-cemented fractures are present in some of the quartz-W veins.

and the dating precision and accuracy by relevant zircon standards was approximately 1% (2σ). Five to seven unknown samples were bracketed with two calibration standards (GJ-1; Jackson et al., 2004) to correct for instrumental mass bias. The sensitivity for measured Pb and U isotopes for a 35 μm spot was typically in the range of 4000 cps/ppm. The Plesovice zircon was also analyzed as a test for the operating conditions to ensure measuring precision and accuracy. Data were processed using the ICPMSDataCal program (Liu et al., 2010). Common lead correction was not performed for most data points $^{206}Pb/^{204}Pb > 1000$. Moreover, $^{204}Pb$ was recorded using an ion counter, and spots with significantly high $^{204}Pb$ content possibly due to the effect of common Pb (e.g. inclusions) were not used for calculations. A Concordia plot of zircon ages was generated using Isoplot 3.0 (Hou et al., 2009). For details of the testing process, please refer to Hou et al. (2009). The analysis of the standard Plesovice samples yielded an age of 338.3 ± 4.5 Ma ($n = 4$, 2σ), while the recommended age is 337.13 ± 0.37 Ma (2σ; Sláma et al., 2008). Both of these ages were concordant within the specified error limit.

### 4.2. Re–Os isotopic analysis

Seven samples of molybdenite samples were collected from the surface and at depth from shafts and drives for Re–Os isotopic analysis. Most of the molybdenite samples came from thin veins, separate blocks from the margins of quartz veins, and the biotite monzogranite.

The Re–Os isotopic analysis was performed at the National Research Center of Geoanalysis in Beijing, China. Refer to Du et al. (2001), Mao et al. (2003b), and Shirey and Walker (1995) for details on the preparation of samples and separation and purification of Re and Os. An ATJA X-series ICP-MS was used to measure the Re–Os isotope ratios, and a Thermo Fisher Scientific ELEMENT 2HR-ICP-MS was used to measure samples with low Re–Os contents. Re isotopes with mass numbers 185 and 187 were selected, and the isotope with mass number 190 was used to monitor Os. Os isotopes with mass numbers 186, 187, 188, 189, 190, and 192 were selected, and the isotope with mass number 185 was used to monitor Re.

### 4.3. Geochemical analysis

The major and trace element analyses of rocks were performed in the Analytical Laboratory at the Beijing Research Institute of Uranium Geology using a Finnigan MATHR-ICP-MS (ELEMENTI), according to the method and reference data specified in the General Rules for ICP-MS Analysis (DZ/T0223–2001). The testing temperature and relative humidity were 20 °C and 30%, respectively.

## 5. Results

### 5.1. Zircon U–Pb age

Zircons used in the study were sampled from the ore-bearing biotite monzogranite. They exhibited well-developed oscillatory zones with no inclusions. They are colourless and transparent or slightly light yellow and irregular granular, tabular or cylindrical shaped with grain diameters ranging from 40 to 150 μm. They are highly automorphic with length to width ratios of 1:2 or 1:3. The CL image shows that the zircons have wide alternated dark and bright rings distributed along the long axis, and the zircon grains generally have regular straight crystal boundaries without irregular cores. The distinct features of the zircons used in this study were all from magmatic crystals without inherited zircons (Claesson et al., 2000; Rayner et al., 2005; Rubatto, 2002). A total of 25 crystal grains were selected for LA-ICP-MS zircon U–Pb dating, and the results are listed in Table 1.

The geochemical data of zircons from the two samples show that Sample DYN-19 has Th and U contents of $86.8 \times 10^{-6}$ – $1388.8 \times 10^{-6}$ and $277.3 \times 10^{-6}$ – $1515.4 \times 10^{-6}$, respectively, and a Th/U ratio of 0.20–1.84. Sample DYN-30 has Th and U contents of $33.5 \times 10^{-6}$ – $3809.7 \times 10^{-6}$ and $173.0 \times 10^{-6}$ – $2008.0 \times 10^{-6}$, respectively, and a Th/U ratio of 0.17–1.82. The zircons from the two samples exhibit some similarity with both having higher Th and U contents, thus yielding darker CL images (Fig. 7).

A total of 16 spots were selected out of the 25 spots obtained from sample DYN-19 for this study, while the other points (DYN-19-1, 3, 4, 10, 13, 14, 16, 23, and 25) were excluded because their $^{206}Pb/^{238}U$ concordances are significantly lower than 90%, owing to their higher contents of common lead. The chosen 16 spots had similar $^{207}Pb/^{206}Pb$, $^{206}Pb/^{238}U$, and $^{207}Pb/^{235}U$ ages. In this study, the zircon crystallization age refers to the $^{206}Pb/^{238}U$ age suitable for their relatively young ages. The $^{206}Pb/^{238}U$ ages of the 16 zircons are within or near a concordant line (Fig. 6a). The Concordia age is 134 ± 1 Ma (MSWD = 0.41), and the $^{206}Pb/^{238}U$ weighted average age is 135 ± 1 Ma. A total of 20 spots were selected from 25 analyzed spots obtained from Sample DYN-30, while the other data points (DYN-30-3, 4, 6, 10, and16) were excluded because of their $^{206}Pb/^{238}U$ concordance is significantly lower than 90%, owing to their higher common lead content. The selected 20 spots had similar $^{207}Pb/^{206}Pb$, $^{206}Pb/^{238}U$, and $^{207}Pb/^{235}U$ ages (Fig. 6b), with a Concordia age of 135 ± 1 Ma (MSWD = 0.52), and a $^{206}Pb/^{238}U$ weighted average age of 135 ± 1 Ma. The two samples have concordant ages within error, and the crystallization age of the biotite monzogranite is interpreted as 135 ± 1 Ma.

### 5.2. Re–Os analysis

The Re–Os isotopic analytical results for the seven samples of molybdenite from the Dayana W-Mo mineralization are listed in Table 2. The Re (5.31–15.38 ppm) and $^{187}Re$ (3.34–9.67 ppm) contents of the seven samples are comparable. Similarly, the Os (0.0262–0.4987 ppb) and $^{187}Os$ (7.378–21.29 ppb) contents also exhibit concordant linear relationships. Therefore, the isochron data points are reasonably apart and suitable for the production of an accurate isochron. Regression analysis of the Re–Os model ages was performed using the equation $t = 1/\lambda[\ln(1 + {}^{187}Os/{}^{187}Re)]$, where λ is the decay constant of $^{187}Re$, $1.666 \times 10^{-11}$ $a^{-1}$ (±1.02%; Smoliar et al., 1996). The results also show that the model ages are concordant and vary within a relatively narrow error range of 130–134 Ma (MSWD = 2.2). The initial Os value is 0.06 ± 0.25, which indicates that the molybdenite contains very little common Os. Therefore, isochron plots and weighted average data were obtained using Isoplot 3, which yield an isochron age of 133 ± 3 Ma and a similar weighted average age of 132 ± 1 Ma (Fig. 8a,b). The isochron and weighted average ages are concordant within the specified error limit, indicating data reliability, and the age of the mineralization is interpreted to be ca. 132 Ma.

### 5.3. Major and trace elements data of the biotite monzogranite

#### 5.3.1. Major elements

The analytical results of major and trace elements of the biotite monzogranite at Dayana are shown in Table 3. Our data suggest that the monzogranite is rich in silica and alkali, with a $SiO_2$ content of 72.84–76.49%, $Na_2O + K_2O$ content of 7.89–9.25%, and $Na_2O/K_2O$ ratios between 0.65 and 1.30, corresponding to the high-K calc-alkaline series (Fig. 9a). The monzogranite is also rich in Al with $Al_2O_3$ contents of 11.7–13.1% and A/CNK values of 1.07–1.44 (typically >1.2), which are characteristics of a strongly peraluminous granite (Fig. 9b). The monzogranite is also relatively poor in Mg assaying 0.03–0.36%.

#### 5.3.2. REE and trace elements

The trace elements (including REE) of the biotite monzogranite at Dayana are listed in Table 3, and normalized plots are shown in Fig. 10. The geochemistry shows that the monzogranite has a low REE content with a ΣREE of $63.68 \times 10^{-6}$ – $94.88 \times 10^{-6}$, and the chondrite normalized REE distribution pattern shows right-inclined distribution (Fig. 10b). In general, the biotite monzogranite is slightly enriched in

**Table 1**
Zircon LA-ICP-MS U–Pb isotopic data for the biotite monzogranite from the Dayana $WO_3$ mineralization of Inner Mongolia.

| Spot# | Th/ $\times10^{-6}$ | U/ $\times10^{-6}$ | Th/U | $^{207}Pb/^{235}U$ Ratio | $^{207}Pb/^{235}U$ 1σ | $^{206}Pb/^{238}U$ Ratio | $^{206}Pb/^{238}U$ 1σ | $^{206}Pb/^{238}U$ Age (Ma) | $^{206}Pb/^{238}U$ 1σ |
|---|---|---|---|---|---|---|---|---|---|
| DYN-19-2 | 336.6 | 1053.2 | 0.32 | 0.1451 | 0.0070 | 0.0210 | 0.0003 | 133.9 | 1.8 |
| DYN-19-5 | 410.3 | 758.6 | 0.54 | 0.1437 | 0.0082 | 0.0213 | 0.0003 | 135.7 | 2.1 |
| DYN-19-6 | 441.1 | 1701.2 | 0.26 | 0.1482 | 0.0095 | 0.0219 | 0.0005 | 139.6 | 3.0 |
| DYN-19-7 | 372.6 | 1425.5 | 0.26 | 0.1458 | 0.0086 | 0.0211 | 0.0004 | 134.4 | 2.4 |
| DYN-19-8 | 179.0 | 911.1 | 0.20 | 0.1480 | 0.0089 | 0.0216 | 0.0004 | 137.7 | 2.5 |
| DYN-19-9 | 130.2 | 576.3 | 0.23 | 0.1524 | 0.0077 | 0.0213 | 0.0004 | 136.0 | 2.5 |
| DYN-19-11 | 550.6 | 1515.4 | 0.36 | 0.1445 | 0.0050 | 0.0213 | 0.0002 | 135.6 | 1.5 |
| DYN-19-12 | 559.6 | 811.6 | 0.69 | 0.1480 | 0.0058 | 0.0213 | 0.0003 | 135.7 | 1.9 |
| DYN-19-15 | 154.9 | 545.4 | 0.28 | 0.1500 | 0.0105 | 0.0217 | 0.0005 | 138.1 | 2.9 |
| DYN-19-17 | 301.5 | 532.1 | 0.57 | 0.1509 | 0.0211 | 0.0212 | 0.0006 | 135.1 | 3.7 |
| DYN-19-18 | 169.0 | 857.4 | 0.20 | 0.1467 | 0.0078 | 0.0216 | 0.0003 | 137.5 | 1.8 |
| DYN-19-19 | 152.7 | 376.7 | 0.41 | 0.1538 | 0.0148 | 0.0214 | 0.0006 | 136.6 | 3.7 |
| DYN-19-20 | 353.5 | 854.6 | 0.41 | 0.1456 | 0.0129 | 0.0209 | 0.0004 | 133.2 | 2.7 |
| DYN-19-21 | 1155.2 | 3703.1 | 0.31 | 0.1494 | 0.0057 | 0.0208 | 0.0004 | 132.4 | 2.3 |
| DYN-19-22 | 520.8 | 1168.5 | 0.45 | 0.1478 | 0.0071 | 0.0214 | 0.0003 | 136.4 | 1.7 |
| DYN-19-24 | 163.5 | 340.5 | 0.48 | 0.1426 | 0.0081 | 0.0211 | 0.0004 | 134.7 | 2.5 |
| DYN-30-1 | 256.3 | 614.3 | 0.42 | 0.1402 | 0.0072 | 0.0207 | 0.0003 | 132.3 | 1.8 |
| DYN-30-2 | 453.5 | 1523.7 | 0.30 | 0.1439 | 0.0060 | 0.0212 | 0.0002 | 135.4 | 1.4 |
| DYN-30-5 | 175.5 | 729.3 | 0.24 | 0.1382 | 0.0150 | 0.0204 | 0.0005 | 129.9 | 3.3 |
| DYN-30-7 | 238.4 | 740.5 | 0.32 | 0.1455 | 0.0077 | 0.0214 | 0.0003 | 136.5 | 2.2 |
| DYN-30-8 | 275.3 | 901.3 | 0.31 | 0.1492 | 0.0102 | 0.0214 | 0.0004 | 136.7 | 2.4 |
| DYN-30-9 | 458.2 | 1292.2 | 0.35 | 0.1405 | 0.0057 | 0.0208 | 0.0003 | 132.5 | 1.6 |
| DYN-30-11 | 500.4 | 1536.6 | 0.33 | 0.1422 | 0.0057 | 0.0211 | 0.0003 | 134.5 | 1.7 |
| DYN-30-12 | 208.9 | 584.7 | 0.36 | 0.1454 | 0.0076 | 0.0210 | 0.0003 | 133.7 | 1.9 |
| DYN-30-13 | 302.6 | 1218.8 | 0.25 | 0.1487 | 0.0061 | 0.0212 | 0.0003 | 135.1 | 1.8 |
| DYN-30-14 | 333.8 | 1092.0 | 0.31 | 0.1468 | 0.0057 | 0.0214 | 0.0003 | 136.4 | 1.9 |
| DYN-30-15 | 367.5 | 1434.1 | 0.26 | 0.1468 | 0.0081 | 0.0210 | 0.0004 | 134.0 | 2.7 |
| DYN-30-17 | 282.2 | 513.4 | 0.55 | 0.1449 | 0.0088 | 0.0213 | 0.0005 | 136.1 | 3.4 |
| DYN-30-18 | 203.9 | 779.8 | 0.26 | 0.1454 | 0.0106 | 0.0210 | 0.0004 | 133.8 | 2.6 |
| DYN-30-19 | 531.4 | 1019.7 | 0.52 | 0.1439 | 0.0060 | 0.0212 | 0.0003 | 135.2 | 1.9 |
| DYN-30-20 | 1136.6 | 1073.4 | 1.06 | 0.1398 | 0.0092 | 0.0208 | 0.0004 | 132.5 | 2.4 |
| DYN-30-21 | 402.3 | 1829.3 | 0.22 | 0.1500 | 0.0047 | 0.0214 | 0.0002 | 136.4 | 1.5 |
| DYN-30-22 | 332.9 | 1184.1 | 0.28 | 0.1509 | 0.0051 | 0.0213 | 0.0003 | 135.6 | 1.7 |
| DYN-30-23 | 374.4 | 1040.7 | 0.36 | 0.1423 | 0.0054 | 0.0209 | 0.0003 | 133.5 | 1.6 |
| DYN-30-24 | 95.7 | 419.3 | 0.23 | 0.1476 | 0.0095 | 0.0214 | 0.0004 | 136.6 | 2.3 |
| DYN-30-25 | 157.8 | 908.7 | 0.17 | 0.1412 | 0.0063 | 0.0209 | 0.0003 | 133.2 | 1.8 |

LREE with an LREE/HREE ratio of 1.31–6.27 and moderate LREE/HREE fractionations. It has an a $(La/Yb)_N$ ratio of 0.58–7.35 and exhibits pronounced negative Eu anomalies with δEu values between 0.04 and 0.45 (Fig. 10b).

The primitive mantle-normalized spider diagram shows that the trace elements have a regular pattern (Fig. 10a) with significantly low Sr content (<400 ppm), and a high Yb content (>2 ppm), indicating that the pressure in the source region was <0.8 or 1 GPa. The Eu anomalies suggest that plagioclase is a residual phase in the source without garnet, and likely at amphibolite facies metamorphic conditions (Martin et al., 2005). The trace elements have a low Nb content (13.4–58.9 ppm) and low Ta content (1.66–24.5 ppm), and a Nb/Ta ratio of 1.45–8.43, which is significantly lower than the ratio range of 16 to 18 for mantle-derived magma (Hofmann, 1988). The monzogranite is clearly enriched in large-ion lithophile elements (LILEs), such as Rb, Th, U, Nd, and Hf, but notably depleted in Ba, Sr, P, Ti, and Nb, with low Ba and Sr contents. This suggests that fractionation was significant at the magmatic source for the monzogranite.

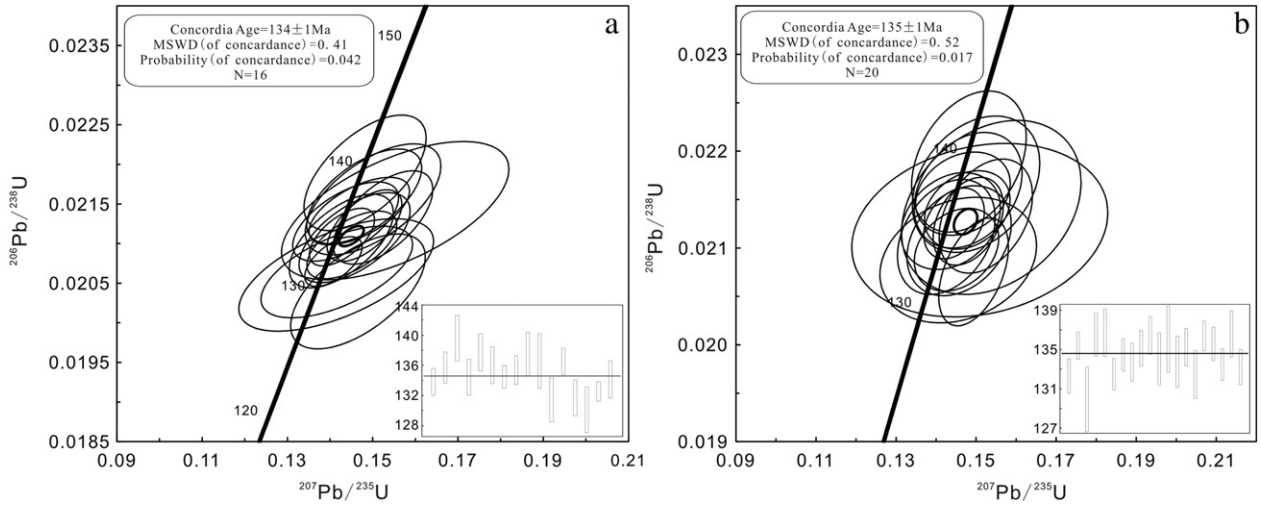


**Fig. 6.** Zircon LA-ICP-MS U–Pb concordia diagrams for the biotite monzogranite at the Dayana W-Mo mineralization.

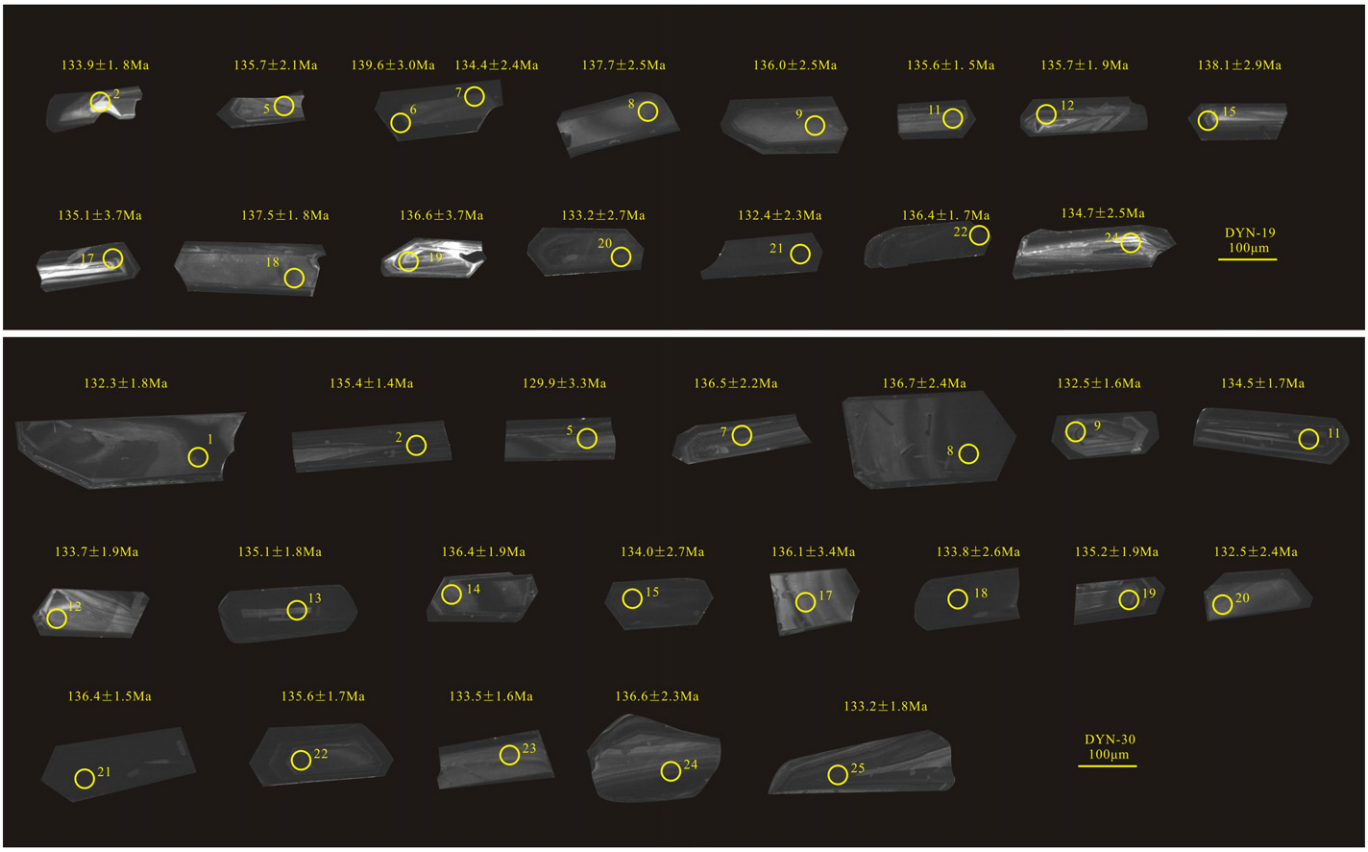


**Fig. 7.** Cathodoluminescence images of zircons from the biotite monzogranite at the Dayana W-Mo deposit. Analyzed spots are circled. Numbers are $^{206}Pb/^{238}U$ age.

## 6. Discussion

### 6.1. Timing of intrusion and mineralization

Previous studies have suggested that the Mesozoic mineralization in the GHMMB formed in discrete periods during 220–240, 160–200 and 125–140 Ma (Mao et al., 2003a; Xu et al., 2015a,b; She et al., 2012). Examples of deposits include some porphyry deposits such as the ca. 230 Ma Badaguan porphyry Cu–Mo deposit (Kang et al., 2014a,b), ca. 178 Ma Wunugetushan porphyry Cu–Mo deposit (Tan et al., 2013; Chen, 2010; Chen et al., 2011), and ca. 140 Ma Shamai quartz vein wolframite deposit (Nie et al., 2010; Jiang et al., in press).

In order to better understand the ore genesis of W and Mo at Dayana, it is necessary to obtain precise geochronological data. The biotite monzogranite at Dayana hosts the W-Mo mineralization towards its upper zones at the contact with shale in the Gegen'aobao Formation, and the mineralization decreases in grade with depth. Exploration at the deposit is continuing, however, the lack of knowledge about the

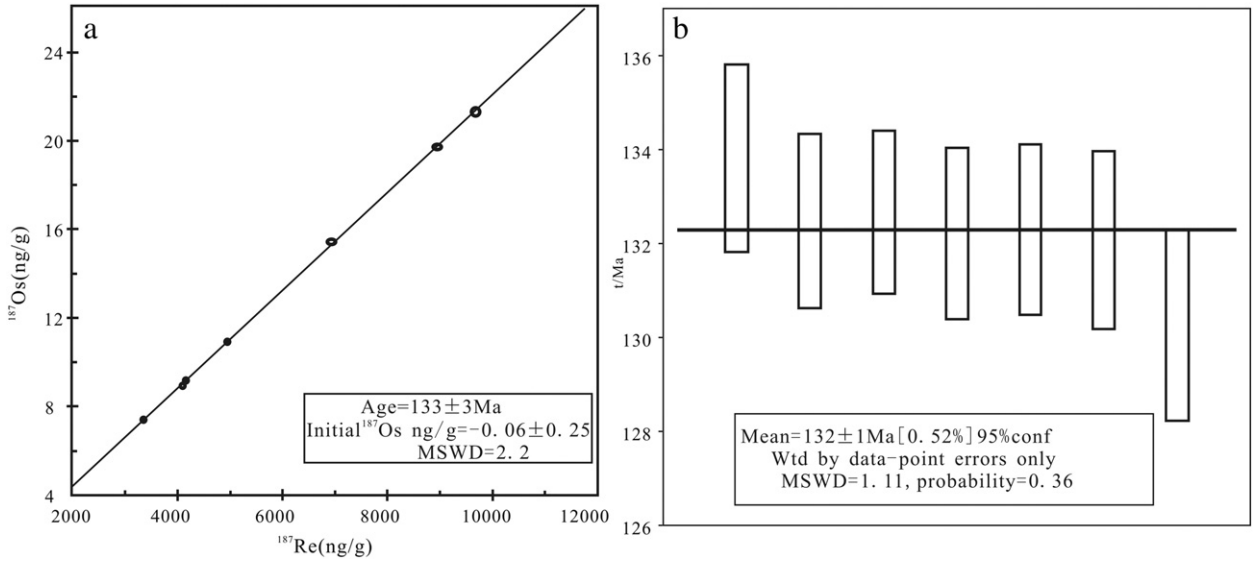


**Fig. 8.** Re–Os isochron diagram for molybdenite (a), and weighted average age (b) of the Dayana W-Mo mineralization.

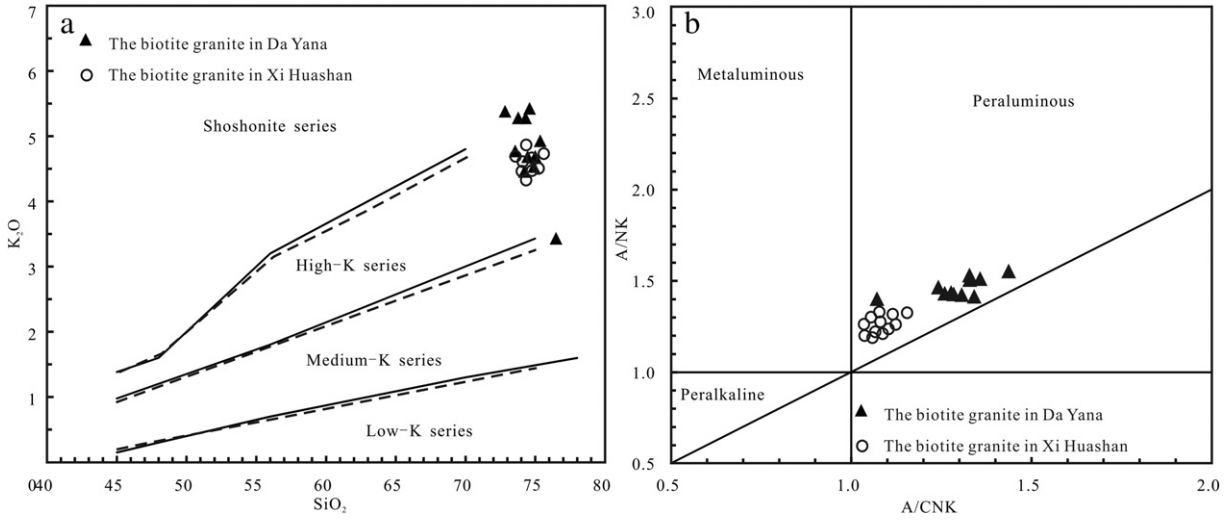


**Fig. 9.** Classifications diagrams for the biotite-monzogranite at the Dayana W-Mo mineralization of Inner Mongolia: (a) $SiO_2$–$K_2O$ plot; and (b) A/NCK-A/NK plot.

genesis of the mineralization has prevented efficient exploration in the region. Based on this study, two samples were collected from the marginal and central areas of the intrusion. The U–Pb dating of zircons yields concordant ages of 134 ± 1 Ma and 135 ± 1 Ma for the samples, which are the same within error. This age is similar to the ca. 140 Ma date recorded for mineralization elsewhere in the belt (Jiang et al., in press).

The geological features discussed about Dayana above indicate that the wolframite and molybdenite are spatially closely associated with each other. They are products of different stages of the same mineralizing event, with molybdenite mineralization relatively preceding the wolframite mineralization.

Seven samples of molybdenite collected from the ores have a Re–Os isochron age of 133 ± 3 Ma. This age is considered robust given that the Re–Os system in the molybdenite remains closed at metamorphic temperatures reaching ~800 °C (e.g. Stein and Bingen, 2002; Bingen and Stein, 2003; Stein et al., 2004; Chen et al., 2011). The date is only slightly younger that the age of the biotite monzogranite suggesting that the monzogranite and mineralization are genetically related. Furthermore, given that the quartz porphyry in the study area intrudes the biotite monzogranite and is crosscut by faults hosting the mineralization in places and crosses the mineralization in other places (Fig. 2), the biotite monzogranite, quartz porphyry, mineralization and faulting must be ca. 133 Ma.

### 6.2. Magma and metal sources

#### 6.2.1. Rock composition

The biotite monzogranite, hosting the W-Mo mineralization at Dayana, is rich in silica (average of 74.5% $SiO_2$), alkali (average of 8.5% $Na_2O + K_2O$) with a corresponding $Na_2O/K_2O$ ratio of 0.78, and 11.7–13.1% $Al_2O_3$, and has an A/CNK value of 1.1–1.4. These values are characteristic of a high-K calc-alkaline magma and a strongly peraluminous granite (Fig. 8). The monzogranite is also poor in Mg (<0.3%). which suggests it is a possible S-type granite, assuming that it is not fractionated (Chappell and White, 1992, 2001). But the trace element characteristics discussed below show that it is fractionated and cannot be strictly called an S-type granite.

The biotite monzogranite has a relatively low total REE content, and its chondrite normalized REE pattern shows right-inclined distribution (Fig. 9). In general, the monzogranite is slightly enriched in LREE with an LREE/HREE ratio of 1.31–6.27 and moderate fractionation in LREE/HREE. It has a low Sr content (<400 ppm) and high Yb content (>2 ppm) with a $(La/Yb)_N$ ratio of 0.58–7.35. It exhibits strong negative Eu anomalies with δEu = 0.04–0.45 (Fig. 9), enriched in LILEs such as Rb, Th, U, Nd, and Hf and notably depleted in Ba, Sr, P, Ti, and Nb. These characteristic define that the Dayana monzogranite as a highly fractionated granite. Meanwhile indicating the presence of residual plagioclase,

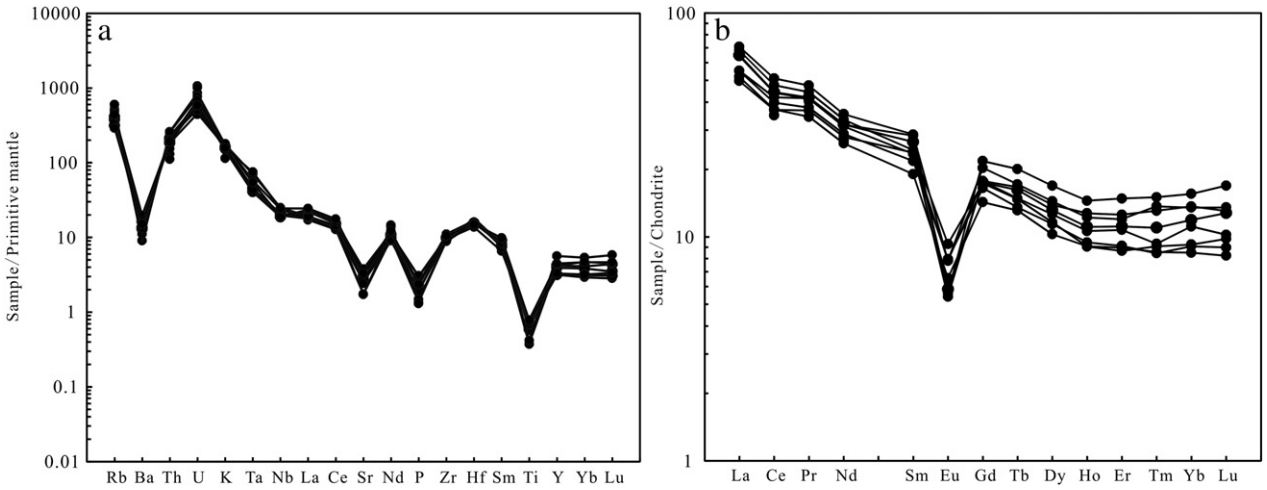


**Fig. 10.** Primitive mantle-normalized spider diagram (a) and chondrite-normalized REE pattern (b) for the biotite monzogranite at the Dayana W-Mo mineralization in Inner Mongolia (normalized values after Sun and Mcdonouch, 1989).

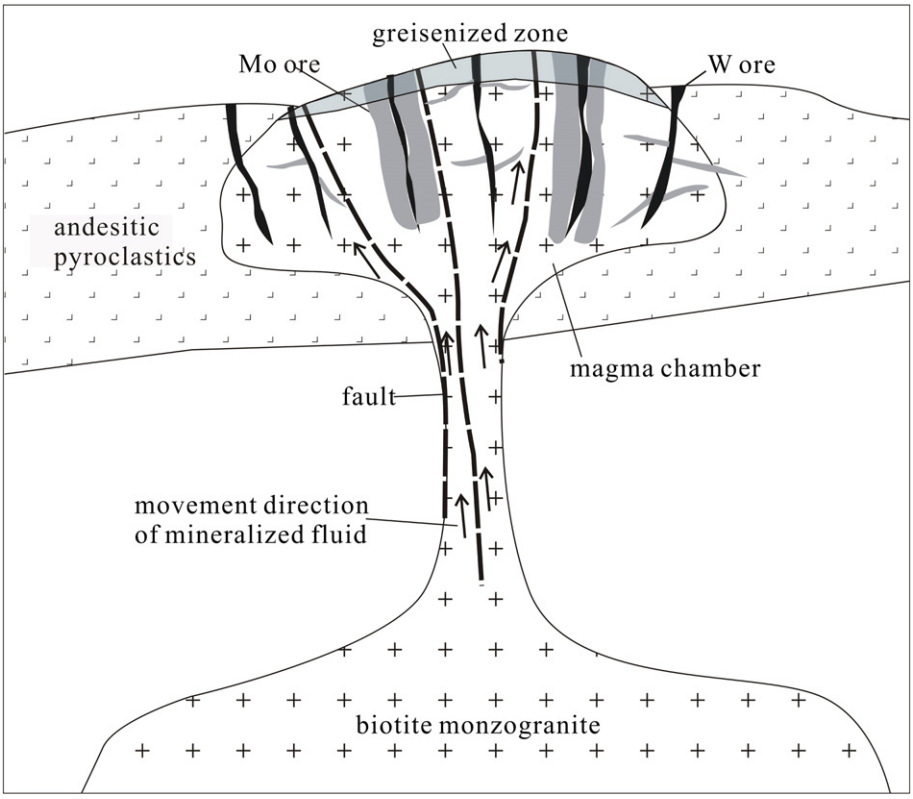


**Fig. 11.** Schematic metallogenic model for the Dayana W-Mo mineralization, Inner Mongolia.

without garnet, at middle crustal (amphibolite facies) levels in the crust with a relatively low forming pressure (<0.8 or 1.0 GPa) (Martin et al., 2005).

Guo et al. (2012) have studied biotite granites hosting wolframite throughout southern China, and have found that most of these granites are high in $SiO_2$ and $Na_2O + K_2O$, are metaluminous to peraluminous, flat or right-inclined distribution patterns of REE and trace elements, distinct negative Eu anomalies, enriched LILEs such as Rb, Th, U, Nd, and Hf, and depleted Ba, Sr, P, Ti, and Nb. These characteristics are similar to that observed at Dayana.

The genesis of the quartz-wolframite mineralization in southern China is proposed to be related to melting of the middle to lower crust following crustal thinning in an extensional setting following continental collision and gravitational collapse (c.f. Guo et al., 2012; Chen and Wang, 2012; Chen et al., 2014; Sun et al., 2009; Xiao et al., 2009; Mao et al., 2009, 2011).

A documented example of quartz-W mineralization in the Greater Hinggan Mountains of Inner Mongolia is the Shamai deposit that is associated with the Shamai Granite (Jiang et al., in press). The Shamai Granite is geochemically similar to the Dayana Granite and similar in age. The Shamai Granite is enriched in LILEs, depleted in high field strength elements (HFSEs) such as Nb and P, has strong negative Eu anomalies ($Eu/Eu^* = 0.02–0.13$), high A/CNK values (1.08–1.40), high Rb/Sr ratios, and is depleted in Ba, Nb, Sr, P and Ti (Jiang et al., in press). The monzogranite and mineralization at Shamai is ca. 150–140 Ma, and the monzogranite originated from the partial melting of a juvenile lower crust in an extensional setting (Jiang et al., in press). This is here considered analogous to the genesis of the Dayana Granite.

### 6.2.2. Metal source

The Re–Os isotopic system can provide important constraints on the age mineralization and a highly sensitive monitor of the possible metal sources (Mao et al., 1999, 2003b, 2008; Foster et al., 1996; Zhang et al., 2005). According to the statistics of numerous Re–Os measurement of molybdenite data (Mao et al., 1999, 2003b, 2008; Foster et al., 1996; Zhang et al., 2005), it is thought that Re concentrations decrease from a mantle to a mixed mantle–crustal and to crustal sources. The decrease is from several hundred ppm in the mantle, to tens of ppm in the mixed mantle–crustal, and to several ppm in the crust. This characteristic of Re has been recognized by many researchers (e.g. Berzina et al., 2005; Li et al., 2007; Selby and Creaser, 2001a,b). At Dayana the Re contents of

**Table 2**
Re–Os isotope data for molybdenite from the Dayana W-Mo mineralization of Inner Mongolia.

| Sample | $W_{(Re)}/\mu g.g^{-1}$ | | $w_{(普Os)}/ng.g^{-1}$ | | $w_{(^{187}Re)}/\mu g.g^{-1}$ | | $w_{(^{187}Os)}/ng.g^{-1}$ | | Model age (Ma) | |
|---|---|---|---|---|---|---|---|---|---|---|
| | M | 2σ | M | 2σ | M | 2σ | M | 2σ | M | 2σ |
| DYN-23 | 10.99 | 0.10 | 0.0262 | 0.0092 | 6.910 | 0.061 | 15.42 | 0.11 | 133.8 | 2.0 |
| DYN-21 | 14.21 | 0.11 | 0.0405 | 0.0099 | 8.928 | 0.071 | 19.73 | 0.12 | 132.5 | 1.8 |
| DYN-74 | 5.305 | 0.034 | 0.0334 | 0.0064 | 3.335 | 0.021 | 7.378 | 0.042 | 132.7 | 1.7 |
| DYN-86 | 7.863 | 0.056 | 0.0359 | 0.0060 | 4.942 | 0.035 | 10.90 | 0.07 | 132.2 | 1.8 |
| DYN-35 | 6.592 | 0.048 | 0.0638 | 0.0073 | 4.143 | 0.030 | 9.142 | 0.057 | 132.3 | 1.8 |
| DYN-37 | 15.38 | 0.12 | 0.0502 | 0.0067 | 9.666 | 0.075 | 21.29 | 0.15 | 132.1 | 1.9 |
| DYN1602–70 | 6.520 | 0.064 | 0.4987 | 0.0699 | 4.098 | 0.040 | 8.901 | 0.063 | 130.2 | 2.0 |

M: Measurement.

**Table 3**
Major elements (wt%), trace elements ($\times 10^{-6}$) composition of the biotite monzogranite at the Dayana W-Mo mineralization, Inner Mongolia.

| Sample | DYN-19 | DYN-30 | DYN-31 | DYN-34 | DYN-45 | DYN-52 | DYN-62 | DYN-76 |
|---|---|---|---|---|---|---|---|---|
| $SiO_2$ | 75.01 | 75.35 | 73.78 | 74.22 | 74.46 | 74.30 | 72.84 | 73.57 |
| $Al_2O_3$ | 12.10 | 11.70 | 12.46 | 12.35 | 12.28 | 12.61 | 12.91 | 12.33 |
| $Fe_2O_{3T}$ | 2.24 | 2.23 | 2.10 | 2.93 | 2.38 | 2.35 | 2.72 | 2.42 |
| CaO | 1.20 | 0.91 | 1.07 | 0.93 | 1.08 | 0.79 | 1.23 | 1.52 |
| MgO | 0.31 | 0.30 | 0.24 | 0.33 | 0.36 | 0.17 | 0.26 | 0.26 |
| $K_2O$ | 4.69 | 4.93 | 5.28 | 4.46 | 4.68 | 5.28 | 5.38 | 4.77 |
| $Na_2O$ | 3.22 | 3.27 | 3.40 | 3.71 | 3.47 | 3.58 | 3.64 | 3.64 |
| MnO | 0.039 | 0.083 | 0.043 | 0.065 | 0.050 | 0.050 | 0.076 | 0.059 |
| $P_2O_5$ | 0.065 | 0.050 | 0.029 | 0.041 | 0.042 | 0.032 | 0.053 | 0.051 |
| $TiO_2$ | 0.13 | 0.15 | 0.081 | 0.15 | 0.15 | 0.091 | 0.16 | 0.17 |
| FeO | 1.43 | 1.79 | 1.36 | 2.05 | 1.65 | 2.20 | 2.43 | 1.88 |
| LOI | 0.49 | 0.42 | 0.58 | 0.29 | 0.34 | 0.10 | 0.17 | 0.20 |
| Total | 100.92 | 101.18 | 100.43 | 101.50 | 100.96 | 101.56 | 101.86 | 100.87 |
| A/CNK | 1.33 | 1.28 | 1.28 | 1.36 | 1.33 | 1.31 | 1.26 | 1.24 |
| A/NK | 1.53 | 1.43 | 1.43 | 1.51 | 1.51 | 1.42 | 1.43 | 1.47 |
| $Na_2O/K_2O$ | 0.69 | 0.66 | 0.65 | 0.83 | 0.74 | 0.68 | 0.68 | 0.76 |
| $Na_2O + K_2O$ | 7.91 | 8.20 | 8.68 | 8.17 | 8.16 | 8.86 | 9.02 | 8.41 |
| La | 15.3 | 15.2 | 11.8 | 12.3 | 13.1 | 13.1 | 16.1 | 16.7 |
| Ce | 27.1 | 27.0 | 22.6 | 22.7 | 24.3 | 25.7 | 29.1 | 31.2 |
| Pr | 3.98 | 3.93 | 3.48 | 3.26 | 3.59 | 3.95 | 4.21 | 4.51 |
| Nd | 14.8 | 14.6 | 13.1 | 12.2 | 13.5 | 14.8 | 15.6 | 16.5 |
| Sm | 4.06 | 3.59 | 3.64 | 2.92 | 3.33 | 4.33 | 3.73 | 4.38 |
| Eu | 0.34 | 0.45 | 0.31 | 0.38 | 0.46 | 0.33 | 0.54 | 0.46 |
| Gd | 3.60 | 3.63 | 3.65 | 2.94 | 3.39 | 4.48 | 3.56 | 4.17 |
| Tb | 0.61 | 0.56 | 0.62 | 0.49 | 0.51 | 0.75 | 0.55 | 0.64 |
| Dy | 3.34 | 3.20 | 3.53 | 2.61 | 2.90 | 4.30 | 2.95 | 3.66 |
| Ho | 0.63 | 0.60 | 0.72 | 0.51 | 0.53 | 0.82 | 0.51 | 0.69 |
| Er | 1.84 | 1.78 | 2.08 | 1.48 | 1.51 | 2.45 | 1.43 | 1.98 |
| Tm | 0.28 | 0.24 | 0.33 | 0.22 | 0.22 | 0.38 | 0.23 | 0.35 |
| Yb | 2.02 | 1.89 | 2.33 | 1.44 | 1.54 | 2.65 | 1.57 | 2.30 |
| Lu | 0.32 | 0.26 | 0.33 | 0.21 | 0.23 | 0.43 | 0.25 | 0.34 |
| ΣREE | 78.31 | 76.85 | 68.47 | 63.68 | 69.08 | 78.48 | 80.37 | 87.98 |
| $(La/Yb)_N$ | 5.44 | 5.76 | 3.63 | 6.11 | 6.07 | 3.55 | 7.35 | 5.23 |
| δEu | 0.27 | 0.38 | 0.26 | 0.39 | 0.42 | 0.22 | 0.45 | 0.32 |
| δCe | 0.83 | 0.83 | 0.85 | 0.86 | 0.86 | 0.87 | 0.85 | 0.86 |
| Li | 71.6 | 72.9 | 52.2 | 59.5 | 43.7 | 58.8 | 77.0 | 56.2 |
| Be | 6.88 | 5.84 | 6.50 | 4.98 | 5.93 | 6.01 | 5.59 | 5.66 |
| V | 35.2 | 31.3 | 40.8 | 33.8 | 33.6 | 32.8 | 30.5 | 28.4 |
| Cr | 25.4 | 23.8 | 38.3 | 24.6 | 28.6 | 39.3 | 24.5 | 24.9 |
| Co | 1.89 | 1.78 | 1.45 | 1.91 | 1.65 | 1.36 | 2.17 | 2.22 |
| Ni | 1.96 | 2.01 | 1.66 | 1.54 | 1.55 | 1.86 | 1.95 | 1.75 |
| Cu | 16.7 | 13.0 | 35.2 | 16.5 | 3.97 | 30.7 | 14.7 | 5.62 |
| Zn | 19.4 | 24.0 | 13.4 | 30.9 | 27.0 | 18.0 | 30.7 | 36.9 |
| Ga | 18.3 | 17.1 | 18.6 | 18.2 | 16.8 | 18.4 | 18.8 | 18.3 |
| Rb | 263 | 239 | 328 | 227 | 199 | 312 | 280 | 184 |
| Sr | 59.0 | 64.8 | 36.4 | 53.6 | 55.3 | 36.8 | 79.9 | 69.6 |
| Y | 19.2 | 17.9 | 19.1 | 14.4 | 14.4 | 25.6 | 15.0 | 20.3 |
| Zr | 112 | 112 | 100 | 106 | 109 | 99.0 | 124 | 118 |
| Nb | 13.6 | 13.4 | 17.1 | 14.0 | 15.0 | 17.9 | 13.5 | 17.4 |
| Cs | 12.4 | 11.9 | 11.9 | 9.55 | 7.15 | 9.25 | 10.6 | 3.95 |
| Hf | 4.66 | 4.83 | 5.59 | 4.25 | 5.24 | 4.73 | 5.17 | 4.58 |
| Ba | 90.5 | 113 | 63.3 | 77.4 | 95.5 | 61.3 | 138 | 106 |
| Ta | 1.68 | 1.89 | 2.36 | 1.66 | 1.85 | 2.87 | 2.22 | 3.07 |
| W | 2.32 | 2.64 | 5.06 | 1.74 | 0.66 | 7.47 | 2.35 | 1.18 |
| Pb | 18.9 | 18.7 | 23.0 | 19.8 | 19.8 | 25.0 | 20.6 | 20.6 |
| Th | 16.8 | 15.6 | 22.0 | 19.4 | 18.2 | 21.9 | 17.2 | 16.3 |
| U | 12.8 | 9.56 | 17.9 | 13.0 | 10.8 | 16.1 | 14.3 | 12.3 |
| Nb/Ta | 8.10 | 7.09 | 7.25 | 8.43 | 8.11 | 6.24 | 6.08 | 5.67 |

molybdenite ranges from 5.3 to 15.4 ppm, which is indicative of a crustal source.

### 6.3. Geodynamic setting

The Mongol-Okhotsk Ocean and the surrounding regions in northern China is thought to have experienced a post-orogenic extensional collapse during the Early Cretaceous, post-arc extensional environment in the wake of the subduction of the paleo-Pacific Plate, or both (Mao and Wang, 1999; Mao et al., 2003a, 2004, 2011; Abzalov, 2007; Li et al., 2007; Guo et al., 2010; Qing et al., 2011, 2012; Wu et al., 2011; She et al., 2012; Li et al., 2013; Ouyang et al., 2013; Wang et al., 2014, 2015; Xu et al., 2013, 2015a,b).

The Dayana W-Mo mineralization is located at the southern part of the Mongol-Okhotsk Ocean in an area that has been affected by Early Cretaceous extension associated with deformation around the Mongol-Okhotsk Ocean and Early Cretaceous compressional events associated with Paleo-Pacific Plate (Mao et al., 2003a; Wu et al., 2011). Evidence for the compressional events in the Dayana area are the presence of conjugate faults and structures hosting the northeast-trending quartz porphyry which, in combination, are indicative of a NE-SW orientated compression. Evidence for the extensional tectonics could be the formation of the granitic magma at middle-crustal levels during ca. 134 Ma. The magma would have carried W-Mo-bearing fluids along conduits such as extensional faults in the crust where the magma

eventually crystalized and followed by the release of ore-forming fluids during ca. 134 Ma.

### 6.4. Exploration potential

The study area is located in a major metallogenic belt in the mid-western part of the Central Asian Orogenic Belt (Mao and Wang, 1999; Mao et al., 2003a, 2011; Xu et al., 2015a,b; Wu et al., 2011; She et al., 2012; Nie et al., 2010; Jiang et al., in press). Numerous Cu, Mo, Pb, Zn, Ag and, recently, W deposits were discovered in the orogen. The Mesozoic metallogenic events in the region around the orogen spanning ca. 200–125 Ma and coeval with various tectonic and magmatic events make the region highly prospective for economic metallic deposits (Mao and Wang, 1999; Hua and Mao, 1999).

In the period following ca. 160 Ma, China's northeastern region was primarily in a post-orogenic extensional regime, which was synchronous with extensional tectonic activities in southern China (Mao and Wang, 1999; Chen and Wang, 2012; Chen et al., 2014; Hua and Mao, 1999). The Lingnan region of southern China is known as the Earth's "Wolframite Town" where numerous quartz-W vein deposits have been discovered (Mao and Wang, 1999; Chen and Wang, 2012; Chen et al., 2014; Hua and Mao, 1999; Guo et al., 2012). Given the tectonic similarities of the Greater Hinggan Mountain and Lingnan regions, exploration activities for the same type of wolframite deposits have not lead to the discovery of W mineralization until recently. This includes the discovery of the large Honghuaerji scheelite deposit (Xiang et al., 2014; Guo et al., 2014), and the recent discovery of the Dayana W-Mo mineralization. This makes the CAOB prospective for various types of deposits including tungsten (and molybdenite) associated with the regional ca. 134 Ma magmatism.

## 7. Conclusions

The studies on the major and trace element exhibited in the paper indicate that the ore-forming biotite monzogranite is rich in silica, alkali and aluminum, poor in magnesium, is characterized by strong negative Eu anomalies, is significantly enriched in LILEs (such as Rb, Th, U, Nd, and Hf), and is notably depleted in Ba, Sr, P, Ti, and Nb. These are characteristics of a highly fractionated peraluminous granite.

The U–Pb zircons dating of samples from the Dayana Granite show that the biotite monzogranite is ca. 134 ± 1 Ma. The Re–Os dating indicates that the mineralization at Dayana is ca. 133 ± 3 Ma. These dates show that both the monzogranite and hosted W-Mo mineralization are coeval within error, are related, and are products of a widespread Cretaceous magmatic event in northern China locally known as the Yanshanian (probably related to widespread post-orogenic extensional collapse during the Cretaceous). Furthermore, the Re content of molybdenite at Dayana ranges from 5.3 to 15.4 ppm, which is indicative of a crustal source.

The ca. 134 Ma biotite monzogranite was emplaced in a succession of andesite, andesitic pyroclastic rocks, dacite, siltstone, and thin beds of mudstone in the Carboniferous-Permian Gegen'aobao Formation. We envision that the ore-forming fluids were derived from highly fractionated magma migrating along penetrative faults and eventually into the Gegen'aobao Formation where W-Mo was concentrated along extensional fractures that are parallel to a NE-trending compressional regime (Fig. 11).

## Acknowledgements

We are grateful to Inner Mongolia Wangsheng Mining Co. Ltd for their invaluable support and cooperation in the fieldwork and data collection for this study. Our thanks will also go to the laboratory staff of the Institute of Mineral Resources of the Chinese Academy of Geological Sciences for their kind assistance in the data measurement and processing for this project.

## References

Abzalov, M., 2007. Zarmitan granitoid-hosted gold deposit, Tian Shan belt, Uzbekistan. Econ. Geol. 102 (3), 519–532.
Berzina, N.A., Sotnikov, V.I., Economou-Eliopoulos, M., Eliopoulos, D.G., 2005. Distribution of rhenium in molybdenite from porphyry Cu–Mo and Mo–Cu deposits of Russia (Siberia) and Mongolia. Ore Geol. Rev. 26, 91–113.
Bingen, B., Stein, H., 2003. Molybdenite Re–Os dating of biotite dehydration melting in the Rogaland high-temperature granulites, S. Norway. Earth Planet. Sci. Lett. 208, 181–195.
Chappell, B.W., White, A.J.R., 1992. I- and S-type granites in the Lachlan Fold Belt. Trans. R. Soc. Edinb. Earth Sci. 83, 1–26.
Chappell, B.W., White, A.J.R., 2001. Two contrasting granite types: 25 years later. Aust. J. Earth Sci. 48, 489–499.
Chen, Z.G., 2010. Mesozoic Tectonic-magmatic Mineralization of Deerbugan Meatallogenic Belt in NE China, and its Geodynamic Setting Ph. D. Dissertation Institute of Geology and Geophysics, Chinese Academy of Sciences, Beijing (in Chinese with English summary).
Chen, Y.C., Wang, D.H., 2012. Four main topics concerning the metallogeny related to Mesozoic magmatism in South China [J]. Geotecton. Metallog. 36 (3), 315–321 (in Chinese with English abstract).
Chen, Z.G., Zhang, L.C., Wan, B., Zhang, Y.T., Wu, H.Y., 2008. Geochemistry and geological significances of ore-forming porphyry with low Sr and Yb value in Wunugetushan copper-molybdenum deposit, Inner Mongolia. Acta Petrol. Sin. 24 (1), 115–128 (in Chinese with English abstract).
Chen, Z.G., Zhang, L.C., Wan, B., Wu, H.Y., Cleven, N., 2011. Geochronology and geochemistry of the Wunugetushan porphyry Cu–Mo deposit in NE China, and their geological significance. Ore Geol. Rev. 43, 92–105.
Chen, Y.C., Wang, D.H., Xu, Z.G., Huang, F., 2014. Outline of regional metallogeny of Ore deposits associated with the Mesozoic magmatism in South China. Geotecton. Metallog. 38 (2), 219–229 (in Chinese with English abstract).
Claesson, S., Vetrin, V., Bayanova, T., Downes, H., 2000. U–Pb zircon age from a Devonian carbonatite dyke, Kola peninsula, Russia: a record of geological evolution from the Archaean to the Palaeozoic. Lithos 51 (1–2), 95–108.
Du, A.D., Zhao, D.M., Wang, S.X., Sun, D.Z., Liu, D.Y., 2001. Precise Re–Os dating for molybdenite by ID-NTIMS with Carius tube sample preparation. Rock Miner. Anal. 20, 247–252 (in Chinese with English abstract).
Foster, J.G., Lambert, D.D., Frick, L.R., 1996. Re–Os isotopic evidence for genesis of Archaean nickel ores from uncontaminated komatiites. Nature 382, 703–706.
Ge, W.C., Wu, F.Y., Zhou, C.Y., Rahman, A.A., 2005. Emplacement age of the Tahe granite and its constraints on the tectonic nature of the Erguna block in the northern part of the Da Hinggan range. Chin. Sci. Bull. 50, 2097–2105.
Ge, W.C., Sui, Z.M., Wu, F.Y., Zhang, J.H., Xu, X.C., Cheng, R.Y., 2007. Zircon U–Pb ages, Hf isotopic characteristics and their implications of the Early Paleozoic granites in the northeastern Da Hinggan Mountains., Northeastern China. Acta Petrol. Sin. 23 (2), 423–440 (in Chinese with English abstract).
Gou, J., Sun, D.Y., Ren, Y.S., Liu, Y.J., Zhang, S.Y., Fu, C.L., Wang, T.H., Wu, P.F., Liu, X.M., 2013. Petrogenesis and geodynamic setting of Neoproterozoic and Late Paleozoic magmatism in the Manzhouli–Erguna area of Inner Mongolia, China: geochronological, geochemical and Hf isotopic evidence. J. Asian Earth Sci. 68, 114–137.
Guo, F., Fan, W.M., Gao, X.F., Li, C.W., Miao, L.C., Zhao, L., Li, H.X., 2010. Sr–Nd–Pb isotope mapping of Mesozoic igneous rocks in NE China: constraints on tectonic framework Phanerozoic crustal growth. Lithos 120, 563–578.
Guo, C.L., Chen, Y.C., Zeng, Z.L., Lou, F.S., 2012. Petrogenesis of the Xihuashan granites in Southeastern China: constraints from geochemistry and in-situ analyses of zircon U–Pb–Hf–O isotopes. Lithos 148, 209–227.
Guo, Z.J., Li, J.W., Huang, G.J., Guan, J.D., Dong, X.Z., Tian, J., Yang, Y.C., She, H.Q., Xiang, A.P., Kang, Y.J., 2014. Sr–Nb–Pb–Hf isotopic characteristics of ore-bearing granites in the Honghuaerji scheelite deposit, Inner Mongolia. Geol. China 04, 1226–1241 (in Chinese with English abstract).
Hofmann, A.W., 1988. Chemical differentiation of the earth: the relationship between mantle, continental crust, and oceanic crust. Earth Planet. Sci. Lett. 90 (3), 297–314.
Hong, D.W., Wang, S.G., Xie, X.L., Zhang, J.S., Wang, T., 2003. Metallogenic province derived from mantle sources: Nd, Sr, S Pb isotope evidence from the Central Asian Orogenic Belt. Gondwana Res. 6, 711–728.
Hou, K.J., Li, Y.H., Tian, Y.Y., 2009. In situ U-Pb zircon dating using laser ablation-multi ion counting-ICP-MS. Mineral Deposits 28 (4), 481–492 (in Chinese with English abstract).
Hua, R.M., Mao, J.W., 1999. A preliminary discussion on the Mesozoic metallogenic explosion in East China. Mineral Deposits 18 (4), 300–307 (in Chinese with English abstract).
Jackson, S.E., Pearson, N.J., Griffin, W.L., Belousova, E.A., 2004. The application of laser ablation-inductively coupled plasma-mass spectrometry to in situ U–Pb zircon geochronology. Chem. Geol. 211 (1–2), 47–69.
Jiang, S.H., Bagas, L., Hu, P., Han, N., Chen, C.L., Liu, Y., Kang, H., 2016. Zircon U–Pb ages and Sr–Nd–Hf isotopes of the highly fractionated granite with tetrad REE patterns in the Shamai tungsten deposit in eastern Inner Mongolia, China: implications for the timing of mineralization and ore genesis. Lithos (in press).
Kang, Y.J., Wang, Y.J., Huang, G.J., She, H.Q., Xiang, A.P., Tian, J., Guo, Z.J., Dong, X.Z., 2014a. Study of rock-forming and ore-forming ages of Badaguan porphyry Cu–Mo deposit in Inner Mongolia. Mineral Deposits 04, 795–806 (in Chinese with English abstract).
Kang, Y.J., She, H.Q., Xiang, A.P., Tian, J., Yang, Y.C., Guo, Z.J., Dong, X.Z., 2014b. Indo Chinese magmatic activity in the Badaguan ore district of Inner Mongolia and its metallogenic implications. Geol. China 04, 1215–1225 (in Chinese with English abstract).
Li, C.W., Guo, F., Fan, W.M., Li, X.Y., 2007. Ar–Ar geochronology of Late Mesozoic volcanic rocks from the Yanji area, NE China tectonic implications. Sci. China Ser. D 54, 505–518.
Li, J.Y., Qu, J.F., Zhang, J., Liu, J.F., Xu, W.L., Zhang, S.H., Guo, R.Q., Zhu, Z.X., Li, Y.P., Li, Y.F., Wang, T., Xu, X.Y., Li, Z.P., Liu, Y.Q., Sun, L.X., Jian, P., Zhang, Y., Wang, L.J., Peng, S.H., Feng, Q.W., Wang, Y., Wang, H.B., Zhao, X.X., 2013. New developments on the reconstruction of Phanerozoic geological history and research of metallogenic geological settings of the Northern China orogenic region. Geol. Bull. China 32 (2/3), 207–219 (in Chinese with English abstract).
Liu, Y.S., Gao, S., Hu, Z.C., Gao, C.G., Zong, K.Q., Wang, D.B., 2010. Continental and oceanic crust recycling-induced melt-peridotite interactions in the *Trans*-North China Orogen: U–Pb dating, Hf isotopes and trace elements in zircons from mantle xenoliths. J. Petrol. 51, 537–571.

Liu, J., Mao, J.W., Wu, G., Luo, D.F., Wang, F., Zhou, Z.H., Hu, Y.Q., 2013. Zircon U–Pb dating for the magmatic rock in the Chalukou porphyry Mo deposit in the northern Great Xing'An Range, China, and its geological significance. Acta Geol. Sin. 87 (2), 208–226 (in Chinese with English abstract).
Liu, Y., Jiang, S.H., Bagas, L., Han, N., Chen, C.L., Kang, H., 2016. Isotopic (C–O–S) geochemistry and Re–Os geochronology of the Haobugao Zn–Fe deposit in Inner Mongolia, NE China. Ore Geol. Rev. 75, 252–267.
Mao, J.W., Wang, Z.L., 1999. A preliminary study on time limits and geodynamic setting of large-scale metallogeny in East China. Mineral Deposits 19 (4), 289–296 (in Chinese with English abstract).
Mao, J.W., Zhang, Z.C., Zhang, Z.H., Du, A.D., 1999. Re–Os isotopic dating of molybdenites in the Xiaoliugou W(−Mo) deposit in the Northern Qilian Mountains and its geological significance. Geochim. Cosmochim. Acta 63 (11–12), 1815–1818.
Mao, J.W., Wang, Y.T., Zhang, Z.H., Yu, J.J., Niu, B.G., 2003a. Geodynamic settings of Mesozoic large-scale mineralization in North China and adjacent areas. Sci. China 46 (8), 839–851.
Mao, J.W., Du, A.D., Sletmann, R., Yu, J.J., 2003b. Re–Os dating for the Shameika porphyry Mo deposit and the Lipovy Log pegmatite rare metal pegmatite, central Urals, Russia. Mineral. Deposita 38, 251–257.
Mao, J.W., Konopelko, D., Seltmann, R., Lehmann, B., Chen, W., Wang, Y.T., Eklund, O., Usubaliev, T., 2004. Post collisional age of the Kumtor gold deposit and timing of Hercynian events in the Tien Shan, Kyrgyzstan. Econ. Geol. 99 (8), 1771–1780.
Mao, J.W., Xie, G.Q., Bierlein, F., Qu, W.J., Du, A.D., Ye, H.S., Pirajno, F., Li, H.M., Guo, B.J., Li, Y.F., Yang, Z.Q., 2008. Tectonic implications from Re–Os dating of Mesozoic molybdenum deposits in the East Qinling–Dabie orogenic belt. Geochim. Cosmochim. Acta 72, 4607–4626.
Mao, J.W., Xie, G.Q., Cheng, Y.B., Chen, Y.C., 2009. Mineral deposit models of Mesozoic Ore deposits in South China. Geol. Rev. 55 (03), 347–354 (in Chinese with English abstract).
Mao, J.W., Pirajno, F., Cook, N., 2011. Mesozoic metallogeny in East China and corresponding geodynamic settings-an introduction to the special issue. Ore Geol. Rev. 43, 1–7.
Martin, H., Smithies, R.H., Rapp, R., Moyen, J.F., Champion, D., 2005. An overview of adakite, tonalite-trondhjemite-granodiorite (TTG), and sanukitoid: relationships and some implications for crustal evolution. Lithos 79 (1–2), 1–24.
Miao, L.C., Liu, D.Y., Zhang, F.Q., Fan, W.M., Shi, Y.R., Xie, H.Q., 2007. Zircon SHRIMPU–Pb ages of the "Xinghuadukou group" in Hanjiayuanzi and Xinlin areas and the "Zhalantun group" in Inner Mongolia, Da Hinggan mountains. Chin. Sci. Bull. 52, 1112–1134.
Nie, F.J., Hu, P., Jiang, S.H., Liu, Y.F., 2010. Geological features, geochronology and origin of the tungsten and tungsten(−molybdenum) deposits in the Shamai-Yuguzer mineralization concentrated camp along the Sino-Mongolian border. Acta Geosci. Sin. 31 (3), 383–394 (in Chinese with English abstract).
Ouyang, H.G., Mao, J.W., Santosh, M., Zhou, J., Zhou, Z.H., Wu, Y., Hou, L., 2013. Geodynamic setting of Mesozoic magmatism in NE China and surrounding regions: perspectives from spatio-temporal distribution patterns of ore deposits. Asian Earth Sci. 78, 222–236.
Qing, M., Ge, L.S., Tang, M.G., Qu, W.J., Yuan, S.S., Zhao, Y.S., 2011. Molybdnite Re–Os isotope age of Bilihe large-size porphyry gold deposit in Sunid Right banner of Inner Mongolia and its geological significance. Mineral Deposits 30 (1), 11–20 (in Chinese with English abstract).
Qing, M., Tang, M.G., Ge, L.S., Han, X.J., Feng, J.B., Yuan, S.S., Zhao, Y.S., 2012. LA-ICP-MS zircon U–Pb age, geochemistry of andesite in Bilihe goldfield, Suniteyouqi, Inner Mongolia and its tectonic significance. Acta Petrol. Sin. 28 (2), 514–524 (in Chinese with English abstract).
Rayner, N., Stern, R.A., Carr, S.D., 2005. Grain-scale variations in trace element composition of fluid-altered zircon, Acasta Gneiss Complex, Northwestern Canada. Contrib. Mineral. Petrol. 148 (6), 721–734.
Rubatto, D., 2002. Zircon trace element geochemistry: partitioning with garnet and the link between U–Pb ages and metamorphism. Chem. Geol. 184, 123–138.
Selby, D., Creaser, R.A., 2001a. Re–Os geochronology and systematics inmolybdenite from the Endako porphyrymolybdenum deposit, British Columbia, Canada. Econ. Geol. 96, 197–204.
Selby, D., Creaser, R.A., 2001b. Late and Mid-Cretaceous mineralization in the Northern Canadian Cordillera: constraints from Re–Os molybdenite dates. Econ. Geol. 96, 1461–1467.
She, H.Q., Li, J.W., Xiang, A.P., Guan, J.D., Zhang, D.Q., Yang, Y.C., Tan, G., Zhang, B., 2012. U–Pb ages of the zircons from primary rocks in middle-northern Daxinganling and its implications to geotectonic evolution. Acta Petrol. Sin. 28 (2), 571–594.
Shirey, S.B., Walker, R.J., 1995. Carius tube digestion for low-blank rhenium–osmium analysis. Anal. Chem. 67, 2136–2141.
Sláma, J., Kosler, J., Condon, D.J., Crowley, J.L., Gerdes, A., Hanchar, J.M., Horstwood, M.S.A., Morris, G.A., Nasdala, L., Norberg, N., Schaltegger, U., Schoene, B., Tubrett, M.N., Whitehouse, M.J., 2008. Plesovice zircon—a new natural reference material for U–Pb and Hf isotopic microanalysis. Chem. Geol. 249, 1–35.
Smoliar, M.I., Walker, R.J., Morgan, J.W., 1996. Re–Os ages of group IIA, IIIA, IVA and VIB iron meteorites. Science 271, 1099–1102.
Song, B., Zhang, Y.H., Wan, Y.S., Jian, P., 2002. Mount making and procedure of the SHRIMP dating. Geol. Rev. 48, 26–30 (in Chinese with English abstract).
Stein, H.J., Bingen, B., 2002. 1.05–1.01 Ga Sveconorwegian metamorphism and deformation of the supracrustal sequence at Sæsvatn, South Norway: Re–Os dating of Cu–Mo mineral occurrences. Geol. Soc. Lond. Spec. Publ. 204, 319–335.
Stein, H.J., Hannah, J.L., Zimmerman, A., Markey, R.J., Sarkar, S.C., Pal, A.B., 2004. A 2.5 Ga porphyry Cu–Mo–Au deposit at Malanjkh and, Central India: implications for Late Archean continental assembly. Precambrian Res. 134, 189–226.
Sun, S.S., McDonough, F., 1989. Chemical and isotopic systematics of oceanic basalt: implications for mantle composition and processes. In: Saunders, A.D., Norry, M.J. (Eds.), Magmatism in the Ocean Basins. Special Publications Geological Society London Vol. 42, pp. 313–345.
Sun, J., Ni, Y.J., Bai, D.Y., Ma, T.Q., 2009. Geochemistry, petrogenesis and tectonic setting of early Yanshanian Yaogangxian granite pluton, Southeastern Hunan Province. Geol. Miner. Resour. South China 03, 12–18 (in Chinese with English abstract).
Sun, L.X., Ren, B.F., Zhao, F.Q., Ji, S.P., Geng, J.Z., 2013. Late Paleoproterozoic magmatic records in the Eerguna massif: evidences from the zircon U–Pb dating of granitic gneisses(in Chinese with english abstract). Geol. Bull. China 32 (2–3), 341–352.
Tan, G., She, H.Q., In, J.P., Yang, Y.C., Li, J.W., Xiang, A.P., Zhang, B., 2013. Source and evolution of ore-fluid in Wunugetushan large Cu–Mo deposit, Inner Mongolia: evidence from fluid inclusions and hydrogen and oxygen isotopic geochemistry. Glob. Geol. 03, 463–482 (in Chinese with English abstract).
Wang, W., Xu, W.L., Wang, F., Meng, E., 2012. Zircon U–Pb chronology and assemblages of Mesozoic granitoids in the Manzhouli-Erguna Area, NE China: constraints on the regional tectonic evolution. Geol. J. China Univ. 18 (1), 88–105 (in Chinese with English abstract).
Wang, J.P., Liu, J.J., Peng, R.M., Liu, Z.J., Zhao, B.S., Li, Z., Wang, Y.F., Liu, C.H., 2014. Gold mineralization in Proterozoic black shales: example from the Haoyaoerhudong gold deposit, northern margin of the North China Craton. Ore Geol. Rev. 63, 150–159.
Wang, T., Guo, L., Zhang, L., Yang, Q., Zhang, J., Tong, Y., Ye, K., 2015. Timing and evolution of Jurassic-cretaceous granitoid magmatisms in the Mongol-Okhotsk belt and adjacent areas, NE Asia: implications for transition from contractional crustal thickening to extensional thinning and geodynamic settings. J. Asian Earth Sci. 97, 365–392.
Wilhem, C., Windley, B.F., Stampfli, G.M., 2012. The Altaids of Central Asia: a tectonic and evolutionary innovative review. Earth Sci. Rev. 113, 3–4.
Wu, F.Y., Sun, D.Y., Ge, W.C., Zhang, Y.B., Grant, M.L., Wilde, S.A., Jahn, B.M., 2011. Geochronology of the Phanerozoic granitoids in Northeastern China. J. Asian Earth Sci. 41, 1–30.
Wu, G., Chen, Y.Ch., Sun, F.Y., Liu, J., Wang, G.R., Xu, B., 2015. Geochronology, geochemistry, and Sr–Nd–Hf isotopes of the early Paleozoic igneous rocks in the Duobaoshan area, NE China, and their geological significance. J. Asian Earth Sci. 97, 229–250.
Xiang, A.P., Yang, Y.C., Li, G.T., She, H.Q., Guan, J.D., Li, J.W., Guo, Z.J., 2012. Diagenetic and metallogenic ages of Duobaoshan porphyry Cu–Mo deposit in Heilongjiang Province. Mineral Deposits 31 (6), 1237–1248 (in Chinese with English abstract).
Xiang, A.P., She, H.Q., Qin, D.J., Wang, Y.J., Han, Z.G., Guan, J.D., Kang, Y.J., 2014. Study on the metallogenic and diagenetic age of Hong-Hua-Er-Ji tungsten polymetallic deposit in Inner Mongolia. Mineral Deposits 02, 428–439 (in Chinese with English abstract).
Xiao, J., Wang, Y., Hong, Y.L., Zhou, Y.Z., Xie, M.H., Wang, D.S., Guo, J.S., 2009. Geochemistry characteristics of Xihuashan tungsten granite and its relationship to tungsten Metallogenesis. J. East China Inst. Technol. 01, 22–31 (in Chinese with English abstract).
Xu, B., Charvet, J., Chen, Y., Zhao, P., Shi, G.Z., 2013. Middle Paleozoic convergent orogenic belts in western Inner Mongolia (China): framework, kinematics, geochronology and implications for tectonic evolution of the central Asian Orogenic Belt. Gondwana Res. 23, 1342–1364.
Xu, B., Song, S., Nie, F., 2015a. The Central Asian Orogenic Belt in Northern China: preface. J. Asian Earth Sci. 97, 179–182.
Xu, B., Zhao, P., Wang, Y.Y., Liao, W., Luo, Z.W., Bao, Z.W., Zhou, Y.H., 2015b. The pre-Devonian tectonic framework of Xing'an-Mongolia orogenic belt (XMOB) in North China. J. Asian Earth Sci. 97, 183–196.
Zhang, Z.H., Cai, F.M., Du, A.D., Zhang, Z.C., Yan, S.H., Yang, J.M., Qu, W.J., Wang, Z.L., 2005. Re–Os dating and ore-forming material tracing of the Karatungk Cu–Ni sulfide deposit in Northern Xinjiang. Acta Petrol. Mineral. 24, 285–293 (in Chinese with English abstract).
Zhang, J.H., Ge, W.C., Wu, F.Y., Wilde, S.A., Yang, J.H., Liu, X.M., 2008. Large-scale Early Cretaceous volcanic events in the northern Great Xing'an range, Northeastern China. Lithos 102, 138–157.